SPECT/CT for Dosimetry

3

Stephan Walrand and Michel Hesse

3.1 Introduction

Likely, most nuclear clinicians will naturally acknowledge that SPECT/CT is the best tool beside PET/CT to get an accurate individual dosimetry in internal radiotherapy. But is it really needed? Often, internal radiotherapies are performed without any real individual dosimetry assessment. So why should we use the state-of-the-art SPECT/CT system?

This practice is linked with two wrong beliefs commonly spread in the nuclear medicine community: increasing the tumours absorbed dose a little bit can just improve a little bit the patient outcome, and the efficacy of external photon beam radiotherapy improved because the irradiation devices improved, so our only option is also to improve our tumour tracers.

The first belief comes from the way we are used to assess the efficacy of internal radiotherapies, i.e. by measuring the change in tumour size or in metabolism a few months after the therapy. And indeed, in this case, increasing a little bit the absorbed dose just increases a little bit the response, as early tissue (organ or tumour) toxicity is a smooth function of the absorbed dose [1–5]; killing a fraction of the tissue cells reduces the tissue metabolism by a similar fraction.

However, late tissue toxicity owns an absorbed dose threshold [6–8]; above a critical fraction of cells killed, the tissue will not be able to recover, and will 'die'. Decay, production of free radicals by ionisation, hits of the radicals to the DNA are all random process. The recovering capacity of a tissue depends on its state. As a result, the normal tissue complication probability (NTCP) and the tumour control probability (TCP) are not step functions, but are quite steeply S-shape functions, i.e. going from 0 to 1 within a few Gy. In addition, the dosimetry of critical organs is highly patient dependent [1]. It is thus of paramount importance to give the maximal activity to the patient that is still safe for him. Indeed, for some patients, the resulting increase in the tumour absorbed dose, even small, could be sufficient to shift from a cancer relapse to a controlled disease. In external beam radiotherapy (EBRT), this feature is called the therapeutic window. Figure 3.1 illustrates this concept applied to ^{90}Y-DOTATOC used in peptide receptor radiotherapy (PRRT). Even if dosimetry assessments are not accurate enough to ensure being in narrow therapeutic windows, the maximal chance

Preamble
Versus the previous 2013 version, recent breakthroughs in the field lead to add 6 new subsections to the "SPECT/CT based dosimetry studies" section, while two new sections have been added to the chapter. The conclusion has thus been fully re-written.

S. Walrand (✉) · M. Hesse
Nuclear Medicine, Université Catholique de Louvain, Brussels, Belgium
e-mail: stephan.walrand@uclouvain.be; michel.hesse@uclouvain.be

H. Ahmadzadehfar et al. (eds.), *Clinical Applications of SPECT-CT*,
https://doi.org/10.1007/978-3-030-65850-2_3

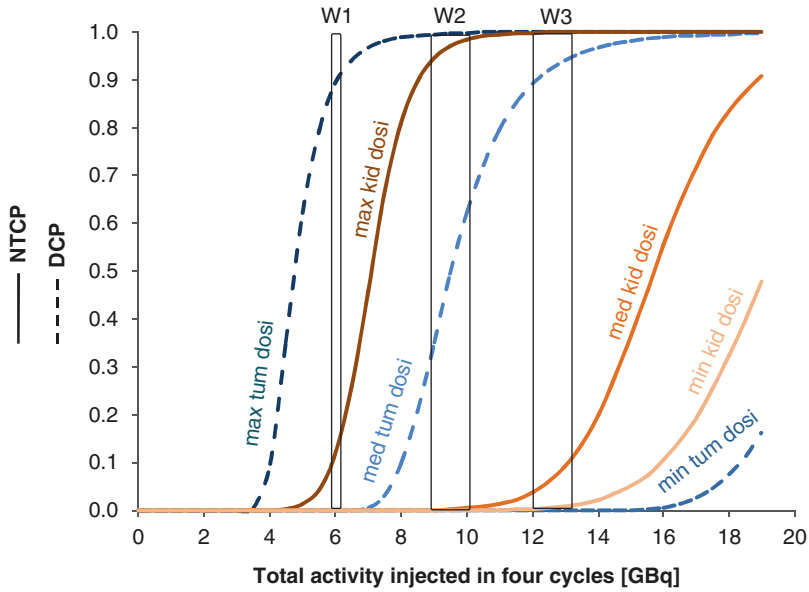

Fig. 3.1 Illustration of the therapeutic windows (TW) concept applied to ^{90}Y-DOTATOC PRRT. The disease control probability (DCP) and kidney NTCP were computed for their respective minimum, median, and maximum dosimetry measured by ^{86}Y-DOTATOC PET in the phase 1 clinical study using amino acid infusion [1, 9]. The curves were computed for a disease owning five tumours, and the tissue radiation tolerance parameters were extracted from [6, 10]. For a patient owning both the median tumour and median kidney dosimetry, W3 is a good TW choice giving a probability of 90% to be curative and of 10% to get a late renal failure. If his tumour dosimetry is the maximal one observed, then W2 is a better choice avoiding any risk of late renal failure. A patient with the maximal kidney dosimetry observed can be cured only if he also owns the maximal tumour dosimetry observed (W1)

for the patient outcome is to be as close as possible to his individual therapeutic window.

During the last decades, the efficacy of EBRT and the sophistication of the devices used have increased together. From these points of view, the recent CyberKnife system is really impressive [11]. In reality, there is no real innovation regarding the CyberKnife hardware (the knife part); it is the combination of a linear accelerator and of a standard industrial 6-axis robot used in car manufacturing, both existing since three decades. So why did this system appear only recently? The major benefit of the CyberKnife is to allow decreasing the absorbed dose to the critical tissues by increasing the number of different beam paths crossing the patient body to target the tumour. This (the cyber part) required motion tracking and an accurate individual treatment planning that uses state-of-the-art multimodality imaging [12–14] including elaborated Monte Carlo simulations of the absorbed dose spreading along the beam paths. This feasibility results from the continuous development of such treatment planning assessment in EBRT during the last decades [15].

Internal radiotherapy had the good fortune to begin with two pathologies owning a large therapeutic window: the radio-synovectomy and the thyroid cancer ^{131}I radio-ablation. These two therapies were used with success by simply injecting a standard activity. Sometimes, an early success durably formats the behaviours, and despite a lot of efforts spent during two decades, no such ideal radio-compound was found for the other cancers. For the patient benefit and also for the long-term future of nuclear medicine, we have to push the available internal radiotherapies to their optimal efficiency by performing an individual treatment planning at the same quality level than that routinely performed in EBRT. This was formalized by the European Union Council in its 2013/59/Euratom directive [16]. That directive equates radionuclide therapies with EBRT regarding the necessity to get dosimetry as precise as possible

to treat patient lesions in an optimized way while preserving healthy tissues. Let emphasize that a dosimetry method displaying a good dose–toxicity correlation on a patient's sample is not sufficient; as the goal is to inject to the patient the maximal activity that he can safely receive, the dosimetry has to be accurate on a patient per patient basis.

3.2 SPECT Versus Planar

There are four effects which definitely disqualify the use of planar-based dosimetry in most of internal radiotherapies: (1) γ-rays attenuation-scatter, (2) tissues overlapping, (3) multi-compartment organ and (4) heterogeneous organ uptake.

1. There is no way to accurately correct gamma-ray attenuation in planar acquisition; use of conjugated planar views, even jointly with a planar transmission scan, is a crude approximation. This method is only valid for an infinitely thin organ without any other activity overlapping. Use of a point scatter kernel to correct for the organs cross-contamination is hampered by the lack of information about the activity depth distribution. This cross-contamination is very cumbersome regarding that biological half-life of the organs is different and that the critical organs can be located close to tissue owning higher activity, such as liver, spleen, tumour, bowels close to the kidneys in PRRT.
2. The critical organs can partially or fully be overlapped by higher taking up tissues. Often, this problem is casually considered and several papers proposed patient dosimetry assessment based on planar views using correction method for the overlapping issues. But to our knowledge, only one [17] presented a validation on phantoms, which should be done for all proposed methods. However, these phantoms were simple: no full overlap, identical effective half-life for the different tissues and no appearing and disappearing activities (bowel in PRRT). Let emphasize that such overlap correction methods have to accurately work for the worst patient case to whom it is not ethically defendable to tell that we cannot do an accurate treatment planning, because we chose to not use the best tool.

   Sandström et al. [18] compared the absorbed dose assessed from conjugate planar views and SPECT/CT in 24 patients imaged 1, 24, 96 and 168 h post ^{177}Lu-DOTATATE therapy. Both modalities were corrected for attenuation; a ^{57}Co transmission scan was performed with the planar modality for this purpose. The planar view to SPECT total kidney absorbed dose ratio ranged from 0.8 to 5.4. Six patients out of 24 had a relative deviation higher than 40%. This clearly disqualifies planar imaging in PRRT pre-therapy planning. Garkavij et al. [19] observed the same problem, in 16 patients also treated with ^{177}Lu-DOTATATE, although with a lower maximal planar view to SPECT total kidney absorbed dose ratio of 1.8. The reason explaining this huge discrepancy between planar and SPECT based dosimetry, in both studies, originated from significant radioactivity overlap as illustrated in Fig. 3.2. In an older ^{90}Y-DOTATOC study, Valkema et al. reported that organs overlapping prevent accurate planar dosimetry assessment underwent in 6 out of 43 patients [20].
3. Some critical organs own several compartments displaying different uptakes, biological washouts, and radiosensitivities. For example, in PRRT, the renal cortex and medulla represent about 70% and 30% of the kidney activity, respectively [21]. The critical tissue, i.e. the glomerular, is located into the cortex. The medulla to cortex S-factor is about one-fourth of that from the cortex to the cortex [22]. The volume, uptake, and biological washout of these compartments are also patient-dependent [1, 23]. These three points require separately assessing the number of decays occurring in the medulla and in the renal cortex, which cannot be done in planar view.
4. Even if the organ has a homogeneous radiosensitivity, i.e. the spatial variations of the radiosensitivity are smaller than the ionizing particle range, such as the liver in ^{90}Y-radioembolization, assessing the intra-

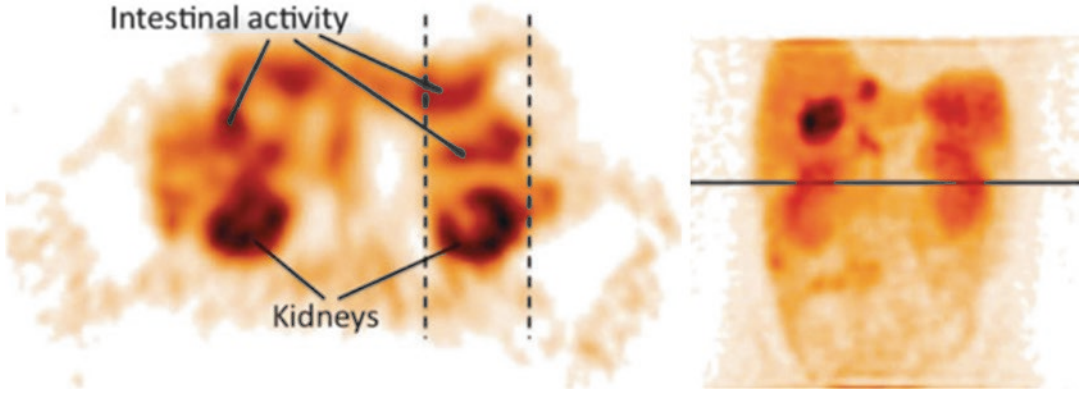

Fig. 3.2 Two images illustrating an imaging situation that results in an overestimated absorbed dose to the kidneys. The activity uptake in the contents of the intestine that overlaps the kidney in the planar image (as indicated by dashed lines) contributes to the absorbed dose, which is not the case in the single-photon emission computed tomography image. Note that the overlapping activity is difficult to detect in the planar images. Reprinted from [19] with permission of John Willey and Sons

organ absorbed dose distribution is still needed. Indeed, studies have shown that the NTCP does not depend only on the mean organ absorbed dose but also on its distribution [24, 25]. NTCP can be calculated using the equivalent uniform dose (EUD) formalism that account for the absorbed dose distribution [10]. For homogeneous density organs, the EUD can be computed based on a fast convolution of the SPECT image by a dose deposition kernel, preferably deconvolved by the SPECT system spatial resolution [26].

Lastly, the argument, which is still sometimes advanced nowadays [17], that planar views have to be used because SPECT is too much time consuming, is not relevant. Irradiating a patient from the inside is a medical act as serious as irradiating him from the outside and should be done in the same sophisticated way.

3.3 SPECT/CT Versus SPECT

Hybrid SPECT/CT system allows a better co-registration accuracy of the two modalities than that obtain by trying to acquire the patient with exactly the same geometry in two different systems or than to use delicate non-rigid fusion. This favourably impacts the activity quantification. Regarding dosimetry assessment, this also helps to link the activity observed to the tissue owning it.

Activity quantification requires the knowledge of the patient attenuation map. SPECT systems equipped with a gamma-ray transmission source are rare. The attenuation map can be derived from the CT Hounsfield values using appropriate rescaling [27]. The issue regarding the additional irradiation received by the patient from the CT performed at the different SPECT time points needed to assess the pharmacokinetics is purely philosophical regarding the four higher order of magnitude of the absorbed dose received during the therapy.

Recent literature review showed that SPECT/CT performed better in absolute quantification than conventional SPECT system [28]. On acquisitions of a torso phantom, Shcherbinin et al. [29] reported errors between 3% and 5% for the isotopes ^{99m}Tc, ^{123}I, ^{131}I, and ^{111}In. The phantom contained two sources centrally and peripherally placed with no surrounding activity. For ^{99m}Tc in a cardiac torso phantom, Vandervoort et al. [30] reported an error of 8% in simulation and within 4% for the acquisition. Both studies included attenuation, scatter and collimator PSF in the iterative reconstruction.

Willowson et al. [31] evaluated SPECT/CT quantification for ^{99m}Tc in phantoms and in

patients. The acquisitions were first corrected for scattering using a transmission-dependent scatter correction (TDSC) method developed on site, and afterwards reconstructed with a commercial OSEM software. The scatter-corrected data, the associated reconstructed data and the co-registered attenuation map were then passed to an iterative Chang attenuation correction algorithm using the CT-derived attenuation correction map. Last, a dead-time correction was performed. In the torso phantom, the relative deviation of the total liver-specific activity assessment was 2%. Clinical evaluation in 12 lung ventilation/perfusion studies after injection of calibrated ^{99m}Tc-MAA activity gave a relative deviation ranging from −7.4 to 3.7% (mean absolute relative deviation of 2.6%).

Beauregard et al. [32] evaluated a commercially available SPECT/CT system in quantitative ^{177}Lu imaging using the manufactory iterative reconstruction algorithm that included CT-based attenuation correction, scatter correction using a triple energy acquisition window and collimator PSF. In addition, they added a camera sensitivity calibration function of the count rate in order to correct for the dead time. They performed seven acquisitions of a 20 cm-diameter phantom with background activity ranging from 0 to 1 GBq including two cylindrical active sources independently ranging from 0 to 0.7 GBq. The deviation activity ranged from −9.5% to 4.1% and from −14.9% to 4.3%, for the whole phantom and for the sources, respectively. The total body activity deviation on five treated patients versus the injected activity (mean ± std. activity = 8.9 ± 0.9 GBq) ranged from −4.9% to 0.0% with dead time correction (from −15.2% to −10.2% without).

Those studies show that SPECT/CT can be used for individualized dosimetry treatment planning. The maximal safe activity found to be injected can be reduce by 10% in order to account for the current quantification accuracy.

Ahmadzadehfar et al. [33] evaluated the impact of ^{99m}Tc-MAA SPECT/CT on SIRT treatment planning and its added value to angiography in 90 studies performed on 76 patients. The accurate co-registration of the two modalities obtained with a hybrid SPECT/CT system allows determining in a robust way which tissue corresponds to the activity observed (Fig. 3.3). Extrahepatic accumulation was detected by planar imaging, SPECT and SPECT/CT in 12%, 17% and 42% of examinations, respectively. The sensitivity for detecting extrahepatic shunting with planar imaging, SPECT and SPECT/CT was 32%, 41% and 100%, respectively, all with a specificity higher than 93%. They concluded that ^{99m}Tc-MAA SPECT/CT is valuable for identifying extrahepatic visceral sites at risk for postradioembolization complications.

3.4 Choice of a Surrogate

^{90}Y is the majorly used radionuclide in internal radiotherapy which does not own any isotope having an appropriated half-life and emitting γ-rays that can be imaged by SPECT. The choice of the good SPECT surrogate is a crucial point which has not yet been sufficiently investigated. ^{90}Y is mainly used in PRRT, radioimmunotherapy and liver radioembolization.

When introducing PRRT, the community thought that tissues uptake should mainly depend on the peptide, perhaps a little bit on the chelator and marginally on the radionuclide which is confined in the chelator cage. Later, Reubi et al. showed that receptor affinity for a same chelator-peptide also strongly depends on the labelled radionuclide [34], e.g. by a factor 2 when replacing Y by Ga in DOTATATE labelling. However, contrary to tumours, organ uptakes are not always only receptor-dependent. For example, an important part of the ^{90}Y-DOTATOC kidney uptake is not receptor-dependent, and ^{111}In-DOTATOC-based dosimetry has shown a good correlation with kidney toxicity post therapy [6].

However, this shows that the choice of a radionuclide surrogate for individualized treatment planning in PRRT requires an initial validation proving identical pharmacokinetics along a patient-per-patient basis. Such studies in PRRT are still lacking. This validation can be performed by imaging the ^{90}Y therapy by bremsstrahlung SPECT or by PET imaging of the compound

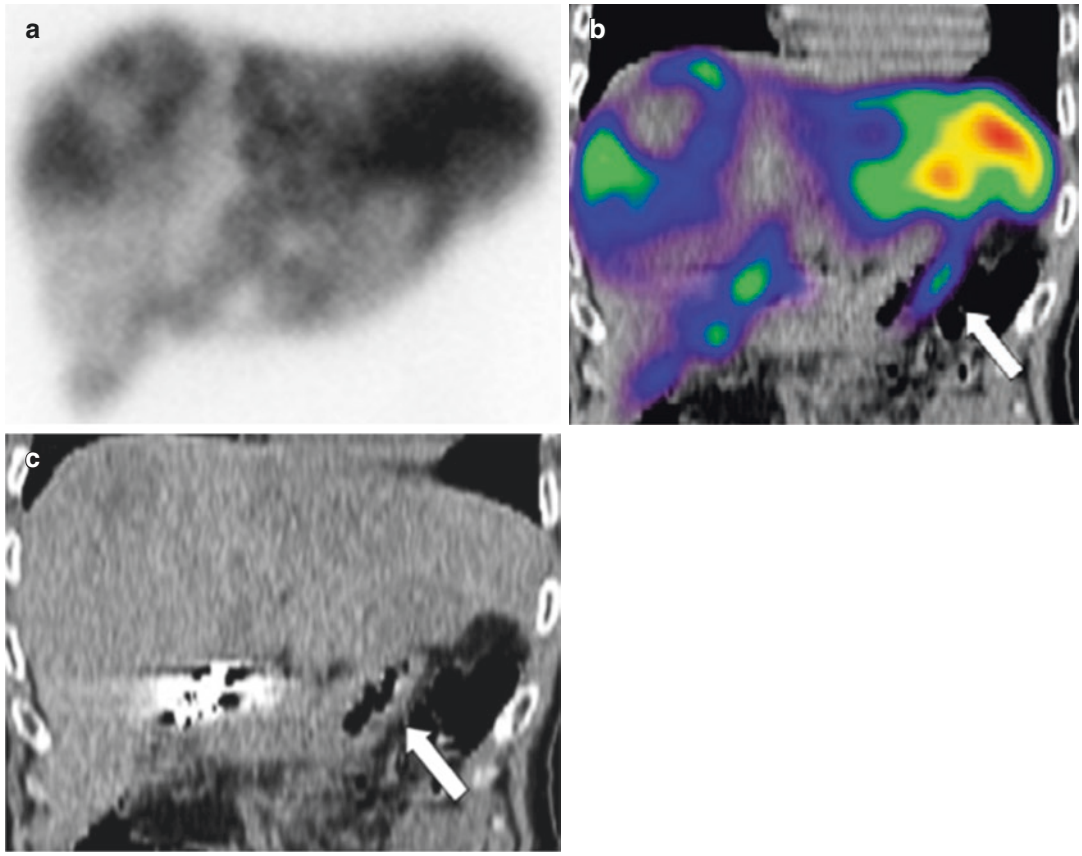

Fig. 3.3 Duodenal accumulation (arrows) in a patient with colorectal cancer, not definable on planar images: planar scan (**a**), SPECT/CT coronal view (**b**), and CT coronal view (**c**). Reprinted from [33] with permission of the Society of Nuclear Medicine

labelled with ^{86}Y [35]; however, both modalities require state-of-the-art correction methods.

In radioimmunotherapy, Minarik et al. [36] compared in three patients the absorbed doses obtained from a pretherapeutic 300 MBq ^{111}In-ibritumomab SPECT/CT to those obtained post ^{90}Y-ibritumomab therapy by bremsstrahlung SPECT/CT using corrections developed on site (see Bremsstrahlung SPECT/CT chapter). The absolute relative differences between absorbed dose computed from ^{111}In and ^{90}Y SPECT/CT were 8.8 ± 13.7 and 8.9 ± 4.0 (mean ± std. in %), for the liver and kidneys, respectively. This supports considering ^{111}In as a surrogate of ^{90}Y in radioimmunotherapy. Compared to peptides, the active site in antibodies is located farther from the radionuclide which likely reduces its impact. However, a validation on a larger patient series is still needed.

For ^{90}Y-loaded glass spheres, Chiesa et al. [25] performed in 35 patients a co-registering of the ^{99m}Tc-MAA SPECT with the ^{90}Y bremsstrahlung SPECT. In the 29 patients treated with the same intentional catheter positioning that in the pretherapeutic study, the biodistribution was markedly different between the two modalities in two patients (7%) and seems only attributable to the different physical properties of spheres and MAA.

For ^{90}Y resin spheres, Jiang et al. [37] conducted an interesting study in 81 paired ^{99m}Tc-MAA and ^{90}Y bremsstrahlung SPECT performed in 75 patients, the catheter being intended to be set in the same position in the two radioemboliza-

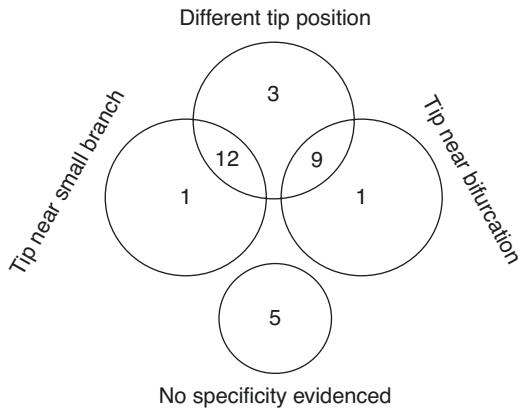

Fig. 3.4 Summary of results from [37] that analyzed in the angiograms the catheter tip position in paired studies showing a segmental perfusion difference (SPD) between ^{99m}Tc-MAA and ^{90}Y SPECT, i.e. 31 out of 81 resin spheres radioembolizations

tions using angiography. They observed a segmental perfusion difference (SPD) between the two SPECT modalities in 31 patients. Analyzing the position of the catheter tip on the two angiograms performed, they noted that 24 SPDs correspond to a different tip position between the two radioembolizations, 2 SPDs occurred with the same tip position, but close to an arterial bifurcation or close to a small branch (Fig. 3.4). However, in 5 SPDs, no particular specificity was evidenced besides the physical properties of the particles.

The correlation dependence on the distance between the catheter tip and the first arterial branch was recently confirmed for ^{90}Y-loaded glass spheres radioembolization in 23 patients [38]. A better correlation was also observed for non-tumoral tissue versus tumours [39, 40].

In a recent study, Smits et al. [41] showed that a ^{166}Ho-scout SPECT/CT performed in the morning of the therapeutic ^{166}Ho radioembolization, itself performed in the afternoon, provided better tumour dose estimation than a ^{99m}Tc-MAA SPECT/CT preformed 4 days earlier. However, it is not clear whether this improvement is attributable to the use of the same device or to the shorter delay with the therapeutic procedure. Good agreement was obtained for both procedures for the non-tumoral dose prediction.

The same team also observed a good agreement for the LSF [42], while ^{99m}Tc MAA systematically exhibited an LSF overestimation likely related to the physical differences between the two devices. Similar overestimation is observed in ^{90}Y-loaded glass spheres radioembolization using ^{99m}Tc-MAA SPECT/CT [43], with the overestimation still being larger using planar imaging [44, 45]. In a phantom study, Kunnen et al. [46] proved dosimetry feasible using a safe 100 MBq ^{90}Y scout activity.

The readers can find a detailed discussion about the challenges of individualized radioembolization therapy using ^{99m}TC-MAA SPECT/CT [47].

3.5 SPECT/CT-Based Dosimetry Studies

3.5.1 Yttrium-90 Spheres Dose–Response

Garin et al. [7] performed a dose–response retrospective study in 36 patients for HCC treated with ^{90}Y-loaded glass spheres. The absorbed doses to liver and tumours were assessed using the ^{99m}Tc-MAA SPECT/CT performed within 1–2 weeks before the therapy and iteratively reconstructed with attenuation and with dual-energy windows scatter correction. The catheter line was counted after therapy in order to estimate the actual injected activity. The planned absorbed dose to the targeted liver volume was 120 Gy based on the MAA, without exceeding 30 Gy for the lungs. Compared to the planning only using the lung shunt and the targeted liver volume, this dose assessment allowed increasing the injected activity in four patients owning large lesions. Mean absorbed doses for non-responding and responding tumours were 124 ± 63 Gy and 328 ± 107 Gy, respectively. The 30 months overall survival evidenced a 205 Gy tumour absorbed dose responding threshold.

Chiesa et al. [48, 49] retrospectively analyzed treatment with ^{90}Y-loaded glass spheres in 52 patients (36, 7 and 9 Child Pugh A5, A6 and B7, respectively). Voxel dosimetry was computed

from the ^{99m}Tc-MAA SPECT performed within 3–4 weeks before the therapy and corrected for attenuation using CT co-registration. All the administrations were lobar, aiming to deliver a mean absorbed dose of 120 Gy to the target lobe including tumour based on the lobe mass measured on CT. There was an overlap in the absorbed doses of the non-responding tumours (0 → 500 Gy) and of the responding tumours (250 → 1500 Gy). Kappadath et al. [50] using ^{90}Y-bremssthralung SPECT/CT-based dosimetry for glass spheres HCC radioembolization in 34 patients also observed such large doses overlap between non-responding and responding tumours.

Strigari et al. [8] retrospectively analyzed HCC treatment with ^{90}Y-resin spheres in 73 patients. The administered activity was determined using the BSA method. Entire liver was treated in 35 patients, a right and left lobar approach was used in 35 and 3 patients, respectively. The liver and tumour dosimetry was assessed on the fusion of the pre-therapeutic ^{99m}Tc-MAA SPECT with a CT using a dedicated software. An elliptical constant attenuation map was used in the SPECT reconstruction with an effective attenuation coefficient of 0.11 cm^{-1} to account for the scatter. The TCP fit, based on RECIST or EASL criteria, showed that two different radio-resistant tumour populations coexisted: 60 and 40% of the tumours had a TD_{50} around a BED of 50 and 130 Gy, respectively. Complete response was observed in all tumours above BED = 200 Gy (AD = 145).

This much higher threshold for tumour response observed in liver-radioembolization studies compared to the traditional 40 Gy observed in EBRT is partly explained by the fact that in internal therapy due to the beta range, the outer shell of the tumour receives about half of the mean absorbed dose.

3.5.2 Yttrium-90 Spheres Dose–Toxicity

In the study [8] summarised here above, Strigari et al. measured a median liver dose of 36 Gy ranging from 6 to 78 Gy. 58, 13 and 2 patients were classified Child-Pugh A, B and C, respectively. The liver was considered as a purely parallel organ (n = 1 in the Lyman–Burman Kutcher model). Liver BED was computed with α/β = 2.5 Gy and using 2.5 h for the sublethal damage repair half-time. The common terminology criteria for adverse events (version 4 National Cancer Institute, Cancer Therapy Evaluation Program) was used to qualify late liver toxicity (4.5 months follow-up). Figure 3.5 shows the liver toxicity–dose relationship considering grades ≥2 as liver toxicity threshold, i.e. at least severe or medically significant.

In the study [48, 49] summarised in the previous section, Chiesa et al. assessed the liver toxicity as the occurrence, during the first 6 months after therapy, of any of: clinically detectable ascites, hepatic encephalopathy, bleeding from oesophageal varices, total bilirubin >3 mg/dL and prothrombin time INR (international normalized ratio) >2.2. Figure 3.6a shows that the NCTP strongly depend on the Child Pugh status. Figure 3.6b shows that for Child Pugh A, the $NCTP_{50}$ occurred around AD = 100 Gy, twofold higher than the AD = 50 Gy observed by Strigari et al. (Fig. 3.5).

Compared to resin spheres, the lower toxicity and efficacy per Gy of the glass one result from a much higher dose distribution heterogeneity as proved by Monte Carlo simulations of spheres transport in hepatic arterial tree [51–53]. d'Abadie et al. [54] taking this heterogeneity into account, using ^{90}Y TOF-PET-based EUD, reunified observed dose–responses between glass spheres, resin spheres and EBRT together.

3.5.3 Yttrium-90 PRRT

Pretherapy dosimetry with ^{86}Y-DOTATOC PET gave impressive renal and bone marrow dose–toxicity correlation in ^{90}Y-DOTATOC therapy [1, 2]. However, its cost, and also the need to infuse amino acids to mimic the therapy, prevent its use in clinical therapy. Fortunately, ^{90}Y-DOTATOC therapy is performed in several cycles in order to reduce the organs toxicity, and thus dosimetry

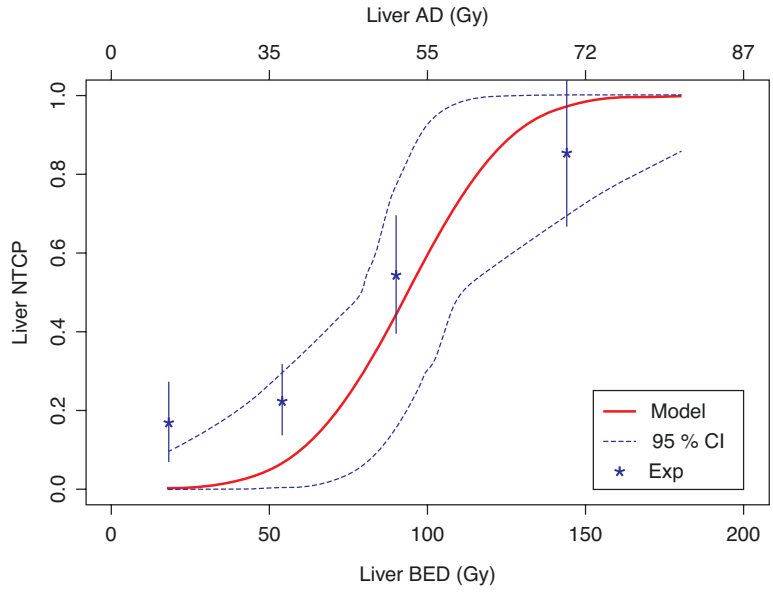

Fig. 3.5 Normal-tissue complication probability of liver toxicity (solid line) vs. liver BED. Dashed-line represents 95% confidence interval. Vertical bars represent SD (caused by number of data in each group that created each point). Exp = experimental data. Reprinted from [8] with authorization of the Society of Nuclear Medicine Liver absorbed dose (AD) was added by the author of the present chapter

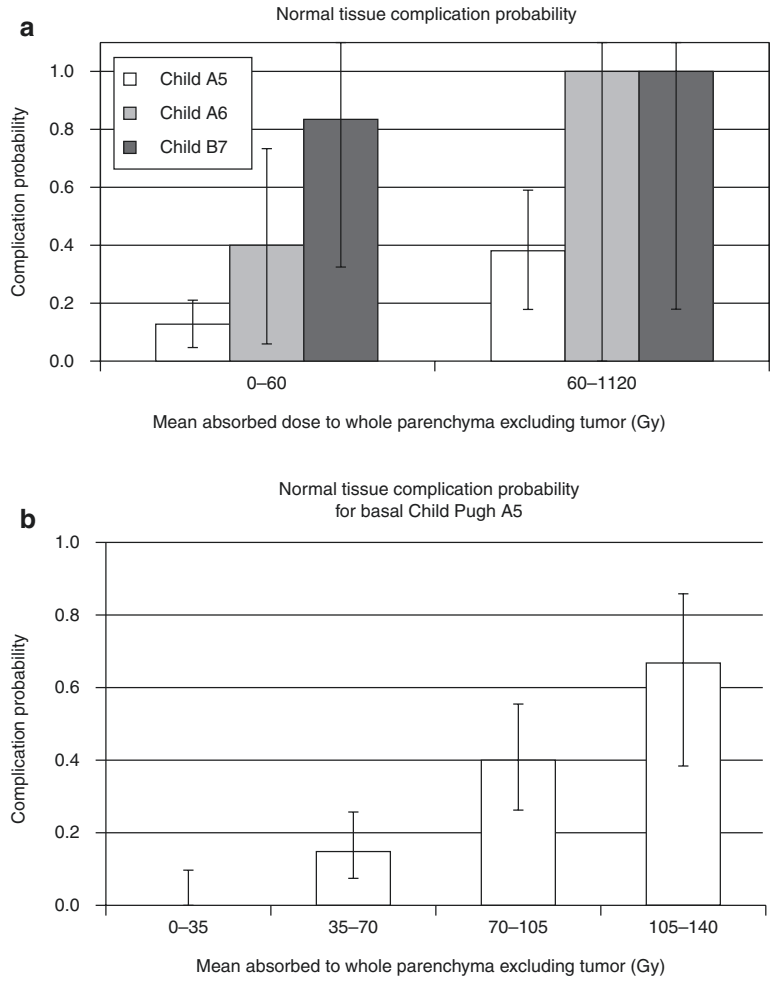

Fig. 3.6 NTCP histogram in function of mean absorbed dose to the lobe excluding tumour for the different Child Pugh populations. Reprinted from [48] with permission of Minerva Medica

performed after one cycle can be used to optimize the activity to be injected in the next one.

Menda et al. [55] conducted a prospective post cycle renal dosimetry using ^{90}Y-bremss. SPECT/CT in 25 patients having neuroendocrine tumours. A ^{90}Y TOF-PET/CT [56] was used at the first time for BREMSS for SPECT/CT calibration purpose. The study confirmed the very high variability of inter-patient renal dosimetry as already observed using ^{86}Y-DOTATOC PET [1], advocating the interest to individually optimize the injected ^{90}Y activity.

3.5.4 Holmium-166

Smits et al. [57] conducted a phase 1 dose-escalation study in ^{166}Ho liver radioembolization with a state-of-the-art design. 6, 3, 3 and 3 patients received activities in order to get a whole-liver absorbed dose of 20, 40, 60 and 80 Gy, respectively, calculated assuming a homogeneous distribution of the activity in the whole liver, i.e. neglecting the tumour liver burden. After coil embolization of undesirable artery branch, ^{99m}Tc-MAA was injected and followed by a SPECT or SPECT/CT imaging. Within 2 weeks, a second angiography was performed with injection of a 250 MBq scout activity of ^{166}Ho spheres followed by a SPECT or SPECT/CT imaging. The same day, a third angiography was performed with injection of the therapeutic ^{166}Ho spheres activity. Both ^{166}Ho radioembolizations intended with the same catheter positioning than that in the ^{99m}Tc-MAA one. SPECT or SPECT/CT and MRI imaging were performed 3–5 post therapy. In all patients, the three SPECT modalities showed similar patterns of the presence or absence of extrahepatic deposition of activity. Regarding the adverse events, the authors concluded that ^{166}Ho radioembolization with a whole-liver dose of 60 Gy is feasible.

In a recent study, the same team showed that it is advocated to use ^{166}Ho-scout SPECT/CT to select patients and to personalize the administered activity in order to target a mean tumour-absorbed dose >90 Gy and a parenchymal dose <55 Gy [58]. In this 40 patients study, only one CTCAE grade 5 related to the radioembolization was observed within the 3 months follow-up, while 90 Gy was the tumour threshold giving a significantly better patients outcome.

Identifying on ^{99m}Tc-MAA SPECT/CT whether the uptake is located in normal liver or tumoral tissue can be highly challenging. Stella et al. [59] conducted a prospective study on 65 ^{166}Ho liver radioembolizations for neuroendocrine metastases. Patients were radioembolized with a scout (n = 29) or a therapeutic (n = 36) ^{166}Ho activity. After the ^{166}Ho SPECT/CT, the patients remained on the camera table and were immediately injected with 50 MBq ^{99m}Tc-stannous phytate which accumulates in Kupffer cells, present in healthy liver tissue, but not in tumorous tissue. Ten minutes after the injection, a triple-energy window SPECT/CT was performed. Dosimetry performed on the ^{166}Ho window SPECT/CT, corrected for ^{99m}Tc cross scattering, was proven sufficiently accurate in VOIs >25 mL for clinical purpose.

3.5.5 Lutetium-177 Antibody

Woliner-van der Weg et al. [60] calculated the bone marrow dosimetry for 13 colorectal cancer patients in ^{177}Lu-labeled di-HSG-peptide therapy. 3D dosimetry was performed on lumbar vertebrae imaged by SPECT/CT at 3, 24 and 72 h after ^{177}Lu administration. 3D dosimetry proved superior in identifying patients at risk of developing any grade of bone marrow toxicity compared to blood- or 2D image-based methods.

In a more recent trial, Blakkisrud et al. [61] studied the bone marrow absorbed dose for 8 non-Hodgkin lymphoma patients treated with ^{177}Lu-lilotomab satetraxetan, with or without additional cold lilotomab. Using SPECT/CT imaging of the L2–L4 vertebrae, they observed that cold lilotomab administration reduced the red-marrow absorbed dose. They also obtained a clear correlation between red-marrow absorbed dose and hematologic toxicity. They concluded that, contrary to some non-imaging method, estimations of bone marrow absorbed dose by

SPECT/CT imaging could be predictive of hematologic adverse events.

3.5.6 Lutetium-177 PRRT

Santoro et al. [62] evaluated the organs at risk in 12 patients treated with ^{177}Lu-DOTATATE using 4 SPECT/CT performed after the first and second cycles. The mean dosimetry for kidney and red marrow was 0.43 ± 0.13 mGy/MBq and 0.04 ± 0.02 mGy/MBq, respectively. As the maximal tolerated dose for red marrow is about tenfold lower than that of kidney [2], this explains why haematological toxicity is the limiting factor in 26% of individually optimized ^{177}Lu PRRT [63].

Hagmarker et al. [64] using the thoracic vertebra activity in ^{177}Lu-DOTATATE SPECT/CT-planar hybrid method found similar red-marrow dosimetry, i.e. 0.06 (0.02–0.12) mGy/MBq in 22 patients without skeletal metastasizes. They observed a dose–toxicity relation (Fig. 3.7) in line with that observed in ^{90}Y-DOTATOC trial using ^{86}Y-DOTATOC PET-based red-marrow dosimetry [2]. In 200 patients, Garsk et al. [63] observed fourfold lower mean blood-based red-marrow dosimetry, i.e. 0.016 mGy/MBq, which was unable to predict the haematological toxicity observed in 40 patients.

Transferrin transchelation [4, 65] is likely the origin of this difference. Indeed, in this binding competition, human transferrin benefits from two major assets versus inorganic chelators:

- Transferring is an active protein: it has two domains, each one containing an anion and a metal binding site. The anion sites act as padlocks: when the metal enter into the metal binding site, the protein geometry changes to enclose the metal which can be released only if a synergic anion binds the appropriate anion binding site [66]. This mechanism ensures that the metal will only be released at an appropriate cell target, e.g. in the red marrow.
- Inorganic chelators have to wait the release of a metal ion by another chelator in order to bind it, which is rare from a good competitor. In contrary, kinetics and spectrometry studies evidenced that transferrin is able to make a ternary (or mixed) complex with the initial metal–chelator complex [67]. During the life of this ternary complex, the metal ion is transferred from the chelator to the transferrin metal binding site.

A recent study in human [68] showed that only 23% and 2% of ^{177}Lu-DOTATATE remain intact after 24 h and 96 h post injection, respectively.

The results of these five studies [60–64] urge for using SPECT/CT in red-marrow dosimetry for all ^{177}Lu therapies and clearly discard the unsuitable blood-based estimation which was although recently used to advocate the useless of dosimetry therapy planning [69].

Ilan et al. [70] observed in ^{177}Lu-DOTATATE therapy of 24 patients, a correlation between tumour volume reduction and three time points

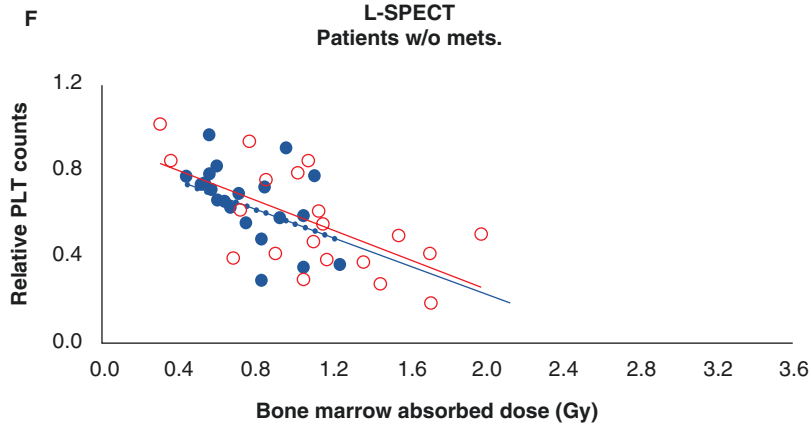

Fig. 3.7 Blue solid circles: relative platelet counts decrease as a function of the hybrid SPECT/CT-planar-based red-marrow dose in ^{177}Lu-DOTATATE therapy (reprinted from [64] with courtesy of Dr. P Bernhardt). Red empty circles: decrease observed in the ^{90}Y-DOTATOC trial using ^{86}Y-DOTATOC PET-based dosimetry added by the authors [2]

SPECT/CT-based absorbed dose. The correlation was remarkably impressive when excluding tumours smaller than 4 cm.

Advances in computational techniques open the way to improved corrections methods for ^{177}Lu SPECT/CT: analytical [71] or MC code [72] to correct for attenuation-scattering and collimator penetration; deep learning algorithm in order to reduce the acquisition time [73].

3.5.7 Iodine-131

Gregory et al. [74] studied the quantitative imaging of ^{123}I and ^{131}I with different SPECT/CT systems. Cylindrical phantoms were used for calibration factors, and 3D-printed phantom mimicking patient's activity distributions were then used to analyze SPECT/CT quantitative imaging. Their results showed that dead-time and calibration factors varied between systems, but that global calibration factors might be used for SPECT/CT from the same manufacturer and with the same crystal size.

Dewaraja et al. [75] in 39 patients with relapsed or refractory non-Hodgkin lymphoma treated with ^{131}I-tositumomab observed a clear separation of progression-free survival for a tumour dose threshold of 2 Gy. Doses were estimated on three time points SPECT/CT using a dose planning MC code. This low-dose threshold is explained by the high radiosensitivity of follicular lymphoma.

3.5.8 Alpha Emitters

Benabdallah et al. [76] evaluated the absolute quantification of ^{223}Ra in bone metastasis therapy. To evaluate the calibration factors, they used the NEMA IEC body phantom with the spheres filled with ^{223}Ra activity concentration ranging from 1.8 to 22.8 kBq/mL. SPECT/CT was performed with a camera equipped with a 5/8″ crystal and triple-energy windows around 85, 154 and 270 keV together with three additional windows for scatter corrections. A TORSO phantom was then used to simulate tumours with tumour to normal tissue ratio close to clinical conditions. They so achieved a quantification of the ^{223}Ra activity with an error smaller than 19%.

3.5.9 SPECT/CT-Based Individualized Therapy Planning

Obsolete medical dogmas are often extremely hard to clear, the most sad stories being the numerous decades needed to implement asepsis in surgery [77] or to treat helicobacter infection in peptic ulcers [78]. Even Louis Pasteur, showing with his microscope the bacteria's present on the lancets, was not able in his lifetime to convince the surgeons to wash their hands and tools between each patient surgery. Nowadays, despite clear evidences [79–81] and in infringement of international authorities recommendations (ICRP 140: first main point, [82]) and rules (Directive 2013/59 Euratom: art. 56, [16]), EANM continue to claim that radionuclide therapy is just similar to chemotherapy, avoiding to mention SPECT/CT in its argumentation [83].

In spite of the abundant literature evidencing strong dose–response and toxicity relationships joined to highly patient-dependent pharmacokinetics here above discussed, this persistent dogma prevented up to recently any randomized trial of individualized therapy planning in molecular radiotherapy. Hopefully, the dynamic and proactive radioembolization community has seriously considered SPECT/CT and, by using it in individualized therapy planning, has evidenced impressive patient outcome improvements [84, 85].

Levillain et al. [84] performed a multicentre retrospective analysis on 58 patients with intrahepatic cholangiocarcinoma treated with ^{90}Y-loaded resin spheres, 47% of them using the empirical BSA methods and 53% using the ^{99m}Tc-MAA SPECT/CT-based partition model. Median overall survival was 14.9 months using the partition model, while was only 5.5 months using the BSA method (Fig. 3.8a). They concluded that SPECT/CT-based personalized activity prescription should be performed.

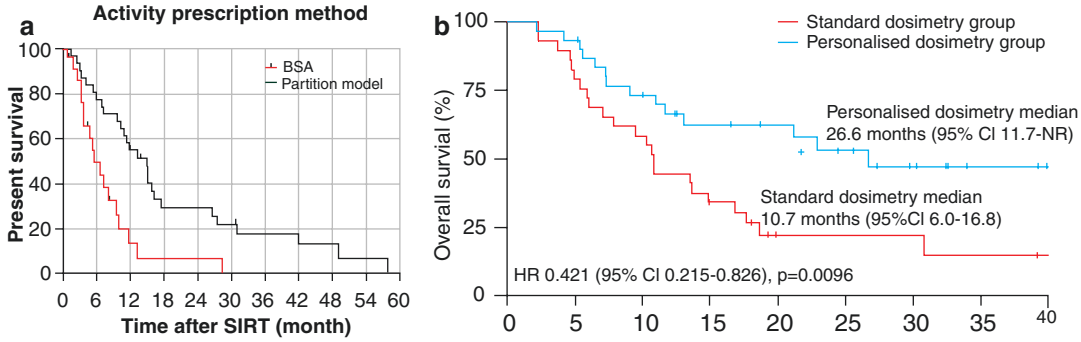

Fig. 3.8 Patients' survival after different liver radioembolization planning. (**a**) Comparison between empirical BSA planning and ^{99m}Tc-MAA SPECT/CT-based partition model (reprinted from [84] with authorization of Springer). (**b**) Comparison between standard dosimetry aiming 120 Gy to the perfused lobe and personalized dosimetry aiming at least 205 Gy in the largest treated tumour, both using ^{99m}Tc-MAA SPECT/CT. (reprinted from [85] with permission of Elsevier)

Garin et al. [85] went one step further in conducting a prospective randomized multicentre phase 2 trial using ^{90}Y-loaded glass spheres in patients with HCC. Outcomes were compared between standard dosimetry aiming 120 Gy to the perfused lobe and personalised dosimetry aiming to deliver at least 205 Gy to the largest treated lesion, both using ^{99m}Tc-MAA SPECT/CT-based dosimetry. The prespecified statistical criterion for stopping early for efficacy occurred after 29 and 31 patients being treated with standard and personalized dosimetry, respectively. Median overall survival was 26.6 months in the personalised dosimetry group, while was only 10.7 months in the standard dosimetry group (Fig. 3.8b).

In parallel to these comparison studies, Del Petre et al. [86], Sundlov et al. [87] and Garske-Roman et al. [63] performed SPECT/CT-based individualized planning ^{177}Lu-DOTATATE therapy in 52, 51 and 200 patients aiming a renal BED = 27Gy, D = 23Gy and D = 23Gy, respectively. They evidenced that applying the standard recommendation of four 7.4GBq-cycles results in undertreating 85, 73 and 49% of the patients.

Garske-Roman et al. [63] observed an impressive progression-free survival (PFS) and overall survival (OS) improvement of patients who were able to reach the 23Gy renal dose limit (n = 114) versus those who cannot due to haematological toxicities (n = 40) (Fig. 3.9).

The patient outcome improvement observed in these individualized therapy planning studies clearly proves the inadequacy of the EANM position on radionuclide therapy [83, 88].

3.5.10 Perspectives: Compton Cameras

Electronic collimation of dual photons emitted in opposite directions makes PET sensitivity and spatial resolution better than those of SPECT by a factor of about 100 and 3, respectively. Early in 1974, such electronics collimation was also proposed for single photon by using a two layers detector [89]. The first layer is optimized to favour Compton scattering while the second is a conventional γ camera that records the scattered gamma-ray. The Compton relation allows deriving information about the incoming direction and energy of the primary gamma-ray (see [90] for a detailed description of camera principles and recent developments).

Compared to SPECT using conventional γ camera, Compton camera has the benefit of a usable wide range of gamma energies from 100 keV to several MeV, of a very large FOV and of allowing SPECT using a few camera positions, and in theory even from a single camera position.

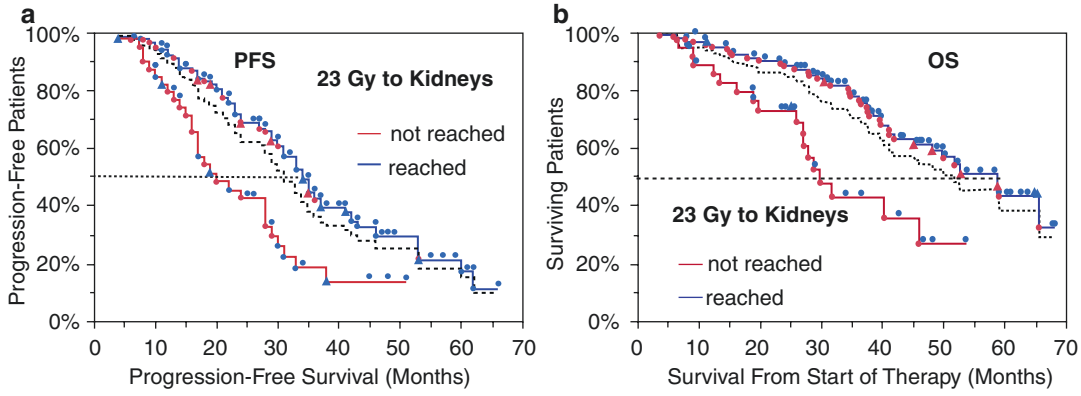

Fig. 3.9 Progression-free survival (**a**) and overall survival (**b**) in ^{177}Lu-DOTA-octreotate therapy in relation to absorbed dose to the kidneys, best morphological response according to RECIST 1.1, and proliferation rate (Ki-67 index) (reprinted from [9] with courtesy of Dr. Sundin)

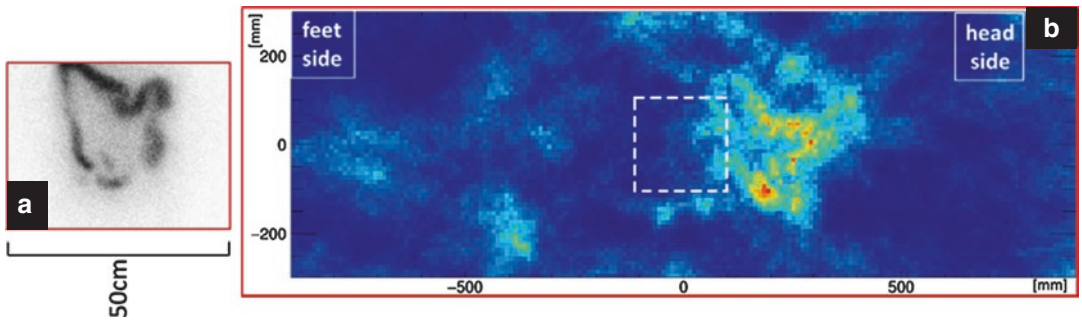

Fig. 3.10 Image of a patient injected with 2.9 MBq of ^{223}Ra (reprinted from [92] with permission of Elsevier). (**a**): 30 min planar acquisition with a MGEP Anger camera. b: whole-body reconstructed slice from a 10 min acquisition using a 22 × 22 cm^2 handheld Compton camera (the left image (**a**) was rotated to respect orientation, and dashed square was added to (**b**) by the authors to visualize the size and position of the camera)

However, during three decades, Compton camera development was hampered by the lack of electronics readout sufficiently transparent to gamma rays in order to use efficient crystals in the first detector layer. This bottle neck was broken in 2002 by the development of thin multi-pixel photo counter (MPPC) [91]. Due to their capability to image a very large FOV in once, compact and mobile Compton cameras development was boosted after 2011 for the Fukushima plan survey using helicopters or drones.

Figure 3.10 shows a whole-body SPECT slice performed post ^{223}Ra therapy using a 22 × 22 cm^2 handheld Compton camera developed for the Fukushima plan survey [92]. A single central camera position of 10 min and 20 cm below the patient table was used. Simultaneous use of several cameras will significantly increase the imaging quality by increasing the sensitivity and the range of sampled gamma-ray directions. As most therapeutic α-emitters, such as ^{223}Ra, ^{225}Ac and ^{211}As, have high energy gamma-ray emitters in their daughters cascade, Compton camera will be the detector of choice in order to perform whole-body 3D dosimetry post α-therapy cycle [93, 94], allowing activity optimization for the next cycles. Obviously, Compton cameras will also be useful for whole-body 3D dosimetry using conventional β-emitters.

3.6 Conclusions

These last 3 years, several dynamics teams implemented SPECT/CT-based individualized planning in ^{90}Y radioembolizations [84, 85] and in

^{177}Lu therapies [63, 86, 87]. Their results clearly proved the high-interpatient dosimetry variations. Impressive patient outcome improvements were also observed. It is extraordinary to notice that all these teams are European, while the EANM persists in claiming that radionuclides therapy is similar to chemotherapy [83], even claiming in infringement of international rules that these therapies can be performed by '*just giving a net activity according to the package insert*' [84], i.e. as such as for conventional drug therapies.

Other recent SPECT/CT studies [62, 64] also cleared the persistent assumption that ^{177}Lu cannot be taken up by the bone marrow in ^{177}Lu-DOTATATE therapy. Indeed, these studies evidenced that the bone marrow dosimetry is about fourfold higher than that estimated using the blood-based method. Such difference was already observed 10 years ago in ^{90}Y-DOTATOC therapy using ^{86}Y-DOTATOC PET-based dosimetry [2, 4]. However, this observation was completely overlooked in the Erasmus phase I/II or in NETTER-1 phase III study, which both considered to only use the inappropriate blood-based method.

No doubt that these breakthroughs in radionuclide therapies will stimulate other teams to move to state-of-the-art dosimetry planning, a strategy which made the success of the external beam radiotherapy.

References

1. Barone R, Borson-Chazot F, Valkema R, Walrand S, Chauvin F, Gogou L, Kvols LK, Krenning EP, Jamar F, Pauwels S. Patient-specific dosimetry in predicting renal toxicity with (90)Y-DOTATOC: relevance of kidney volume and dose rate in finding a dose-effect relationship. J Nucl Med. 2005;46:99S–106S.
2. Pauwels S, Barone R, Walrand S, Borson-Chazot F, Valkema R, Kvols LK, Krenning EP, Jamar F. Practical dosimetry of peptide receptor radionuclide therapy with (90)Y-labeled somatostatin analogs. J Nucl Med. 2005;46:92S–8S.
3. Walrand S, Lhommel R, Goffette P, Van den Eynde M, Pauwels S, Jamar F. Hemoglobin level significantly impacts the tumor cell survival fraction in humans after internal radiotherapy. EJNMMI Res. 2012;2:20.
4. Walrand S, Barone R, Pauwels S, Jamar F. Experimental facts supporting a red marrow uptake due to radiometal transchelation in 90Y-DOTATOC therapy and relationship to the decrease of platelet counts. Eur J Nucl Med Mol Imaging. 2011;38(7):1270–80.
5. Flamen P, Vanderlinden B, Delatte P, Ghanem G, Ameye L, Van Den Eynde M, Hendlisz A. Multimodality imaging can predict the metabolic response of unresectable colorectal liver metastases to radioembolization therapy with Yttrium-90 labeled resin spheres. Phys Med Biol. 2008;53(22):6591–603.
6. Wessels BW, Konijnenberg MW, Dale RG, Breitz HB, Cremonesi M, Meredith RF, Green AJ, Bouchet LG, Brill AB, Bolch WE, Sgouros G, Thomas SR. MIRD pamphlet no. 20: the effect of model assumptions on kidney dosimetry and response—implications for radionuclide therapy. J Nucl Med. 2008;49(11):1884–99.
7. Garin E, Lenoir L, Rolland Y, Edeline J, Mesbah H, Laffont S, Porée P, Clément B, Raoul JL, Boucher E. Dosimetry based on 99mTc-macroaggregated albumin SPECT/CT accurately predicts tumor response and survival in hepatocellular carcinoma patients treated with 90Y-loaded glass spheres: preliminary results. J Nucl Med. 2012;53(2):255–63.
8. Strigari L, Sciuto R, Rea S, Carpanese L, Pizzi G, Soriani A, Iaccarino G, Benassi M, Ettorre GM, Maini CL. Efficacy and toxicity related to treatment of hepatocellular carcinoma with 90Y-SIR spheres: radiobiologic considerations. J Nucl Med. 2010;51(9):1377–85.
9. Jamar F, Barone R, Mathieu I, Walrand S, Labar D, Carlier P, de Camps J, Schran H, Chen T, Smith MC, Bouterfa H, Valkema R, Krenning EP, Kvols LK, Pauwels S. ^{86}Y-DOTA^{0}-D-Phe1-Tyr3-octreotide (SMT487)—a phase 1 clinical study: pharmacokinetics, biodistribution and renal protective effect of different regimens of amino acid co-infusion. Eur J Nucl Med Mol Imaging 2003;30(4):510–518.
10. Gay HA, Niemierko A. A free program for calculating EUD-based NTCP and TCP in external beam radiotherapy. Phys Med. 2007;23:115–25.
11. Adler JR, Chang SD, Murphy MJ, Doty J, Geis P, Hancock SL. The Cyberknife: a frameless robotic system for radiosurgery. In: Stereotactic and functional neurosurgery. 1997;69:124–8.
12. Devic S. MRI simulation for radiotherapy treatment planning. Med Phys. 2012;39(11):6701–11.
13. Scripes PG, Yaparpalvi R. Technical aspects of positron emission tomography/computed tomography in radiotherapy treatment planning. Semin Nucl Med. 2012;42(5):283–8.
14. Götz L, Spehl TS, Weber WA, Grosu AL. PET and SPECT for radiation treatment planning. Q J Nucl Med Mol Imaging. 2012;56(2):163–72.
15. Taylor ML, Kron T, Franich RD. A contemporary review of stereotactic radiotherapy: inherent dosimetric complexities and the potential for detriment. Acta Oncol. 2011;50(4):483–508.
16. https://eur-lex.europa.eu/legal-content/EN/TXT/?uri=CELEX%3A32013L0059

17. Berker Y, Goedicke A, Kemerink GJ, Aach T, Schweizer B. Activity quantification combining conjugate-view planar scintigraphies and SPECT/CT data for patient-specific 3-D dosimetry in radionuclide therapy. Eur J Nucl Med Mol Imaging. 2011;38(12):2173–85.
18. Sandström M, Garske U, Granberg D, Sundin A, Lundqvist H. Individualized dosimetry in patients undergoing therapy with (177)Lu-DOTA-D-Phe (1)-Tyr (3)-octreotate. Eur J Nucl Med Mol Imaging. 2010;37(2):212–25.
19. Garkavij M, Nickel M, Sjögreen-Gleisner K, Ljungberg M, Ohlsson T, Wingårdh K, Strand SE, Tennvall J. 177Lu-[DOTA0,Tyr3] octreotate therapy in patients with disseminated neuroendocrine tumors: Analysis of dosimetry with impact on future therapeutic strategy. Cancer. 2010;116(4):1084–92.
20. Valkema R, Pauwels S, Kvols LK, Kwekkeboom DJ, Jamar F, de Jong M, et al. Long-term follow-up of renal function after peptide receptor radiation therapy with 90Y-DOTA0, Tyr3-octreotide and 177Lu-DOTA0, Tyr3-octreotate. J Nucl Med. 2005;46:83S–91.
21. Konijnenberg M, Melis M, Valkema R, Krenning E, de Jong M. Radiation dose distribution in human kidneys by octreotides in peptide receptor radionuclide therapy. J Nucl Med. 2007;48(1):134–42.
22. Bouchet LG, Bolch WE, Blanco HP, Wessels BW, Siegel JA, Rajon DA, Clairand I, Sgouros G. MIRD pamphlet no 19: absorbed fractions and radionuclide S values for six age-dependent multiregion models of the kidney. J Nucl Med. 2003;44(7):1113–47.
23. De Jong M, Valkema R, Van Gameren A, et al. Inhomogeneous localization of radioactivity in the human kidney after injection of [111In-DTPA]octreotide. J Nucl Med. 2004;45:1168–71.
24. Cremonesi M, Ferrari M, Bartolomei M, Orsi F, Bonomo G, Aricò D, Mallia A, De Cicco C, Pedroli G, Paganelli G. Radioembolisation with 90Y-spheres: dosimetric and radiobiological investigation for multi-cycle treatment. Eur J Nucl Med Mol Imaging. 2008;35(11):2088–96.
25. Chiesa C, Maccauro M, Romito R, Spreafico C, Pellizzari S, Negri A, Sposito C, Morosi C, Civelli E, Lanocita R, Camerini T, Bampo C, Bhoori S, Seregni E, Marchianò A, Mazzaferro V, Bombardieri E. Need, feasibility and convenience of dosimetric treatment planning in liver selective internal radiation therapy with (90)Y spheres: the experience of the National Tumor Institute of Milan. Q J Nucl Med Mol Imaging. 2011;55(2):168–97.
26. Lhommel R, van Elmbt L, Goffette P, Van den Eynde M, Jamar F, Pauwels S, Walrand S. Feasibility of 90Y TOF PET-based dosimetry in liver metastasis therapy using SIR-spheres. Eur J Nucl Med Mol Imaging. 2010;37(9):1654–62.
27. Brown S, Bailey DL, Willowson K, Baldock C. Investigation of the relationship between linear attenuation coefficients and CT Hounsfield units using radionuclides for SPECT. Appl Radiat Isot. 2008;66(9):1206–12.
28. Ritt P, Vija H, Hornegger J, Kuwert T. Absolute quantification in SPECT. Eur J Nucl Med Mol Imaging. 2011;38:S69–77.
29. Shcherbinin S, Celler A, Belhocine T, Vanderwerf R, Driedger A. Accuracy of quantitative reconstructions in SPECT/CT imaging. Phys Med Biol. 2008;53:4595–604.
30. Vandervoort E, Celler A, Harrop R. Implementation of an iterative scatter correction, the influence of attenuation map quality and their effect on absolute quantitation in SPECT. Phys Med Biol. 2007;52:1527–45.
31. Willowson K, Bailey DL, Baldock C. Quantitative SPECT reconstruction using CT-derived corrections. Phys Med Biol. 2008;53(12):3099–112.
32. Beauregard JM, Hofman MS, Pereira JM, Eu P, Hicks RJ. Quantitative (177)Lu SPECT (QSPECT) imaging using a commercially available SPECT/CT system. Cancer Imaging. 2011;11:56–66.
33. Ahmadzadehfar H, Sabet A, Biermann K, Muckle M, Brockmann H, Kuhl C, Wilhelm K, Biersack HJ, Ezziddin S. The significance of 99mTc-MAA SPECT/CT liver perfusion imaging in treatment planning for 90Y-sphere selective internal radiation treatment. Nucl Med. 2010;51(8):1206–12.
34. Reubi JC, Schär JC, Waser B, Wenger S, Heppeler A, Schmitt JS, Mäcke HR. Affinity profiles for human somatostatin receptor subtypes SST1-SST5 of somatostatin radiotracers selected for scintigraphic and radiotherapeutic use. Eur J Nucl Med. 2000;27(3):273–82.
35. Walrand S, Flux GD, Konijnenberg MW, Valkema R, Krenning EP, Lhommel R, Pauwels S, Jamar F. Dosimetry of yttrium-labelled radiopharmaceuticals for internal therapy: 86Y or 90Y imaging? Eur J Nucl Med Mol Imaging. 2011;38:S57–68.
36. Minarik D, Sjögreen-Gleisner K, Linden O, Wingårdh K, Tennvall J, Strand SE, Ljungberg M. 90Y bremsstrahlung imaging for absorbed-dose assessment in high-dose Radioimmunotherapy. J Nucl Med. 2010;51:1974–8.
37. Jiang M, Fischman A, Nowakowski FS, Heiba S, Zhang Z, Knesaurek K, Weintraub J, Josef MJ. Segmental perfusion differences on paired Tc-99m macroaggregated albumin (MAA) hepatic perfusion imaging and Yttrium-90 (Y-90) bremsstrahlung imaging studies in SIR-sphere Radioembolization: associations with angiography. J Nucl Med Radiat Ther. 2012;3:1.
38. Kafrouni M, Allimant C, Fourcade M, Vauclin S, Guiu B, Mariano-Goulart D, Bouallègue FB. Analysis of differences between 99m Tc-MAA SPECT-and 90 Y-microsphere PET-based dosimetry for hepatocellular carcinoma selective internal radiation therapy. EJNMMI Res. 2019;9:62.
39. Gnesin S, Canetti L, Adib S, Cherbuin N, Monteiro MS, Bize P, Denys A, Prior JO, Baechler S, Boubaker A. Partition model–based 99mTc-MAA SPECT/CT predictive dosimetry compared with 90Y TOF PET/CT posttreatment dosimetry in Radioembolization of hepatocellular carcinoma: a quantitative agreement comparison. J Nucl Med. 2016;57:1672–8.
40. Jadoul A, Bernard C, Lovinfosse P, Gérard L, Lilet H, Cornet O, Hustinx R. Comparative dosimetry

between 99m Tc-MAA SPECT/CT and 90 Y PET/CT in primary and metastatic liver tumors. Eur J Nucl Med Mol Imag. 2020;47(4):828–37.
41. Smits ML, Dassen MG, Prince JF, Braat AJ, Beijst C, Bruijnen RC, de Jong HW, Lam MG. The superior predictive value of 166 ho-scout compared with 99m Tc-macroaggregated albumin prior to 166 ho-microspheres radioembolization in patients with liver metastases. Eur J Nucl Med Mol Imag. 2019;9:1–9.
42. Elschot M, Nijsen JF, Lam MG, Smits ML, Prince JF, Viergever MA, van den Bosch MA, Zonnenberg BA, de Jong HW. 99m Tc-MAA overestimates the absorbed dose to the lungs in radioembolization: a quantitative evaluation in patients treated with 166 ho-microspheres. Eur J Nucl Med Mol Imaging. 2014;41:1965–75.
43. Song YS, Paeng JC, Kim HC, Chung JW, Cheon GJ, Chung JK, Lee DS, Kang KW. PET/CT-based dosimetry in 90Y-microsphere selective internal radiation therapy: single cohort comparison with pretreatment planning on 99mTc-MAA imaging and correlation with treatment efficacy. Medicine. 2015;94(23):e945.
44. Mauxion T, Hobbs R, Herman J, Lodge M, Yue J, Du Y, Wahl R, Geschwind JF, Frey E. Comparison of lung shunt fraction (LSF) from pre-therapy 99mTc MAA and post-therapy quantitative 90Y imaging in microsphere (MS) radioembolization. J Nucl Med. 2015;56:104.
45. Allred JD, Niedbala J, Mikell JK, Owen D, Frey KA, Dewaraja YK. The value of 99m Tc-MAA SPECT/CT for lung shunt estimation in 90 Y radioembolization: a phantom and patient study. Eur J Nucl Med Mol Imaging Res. 2018;8:50.
46. Kunnen B, Dietze MM, Braat AJ, Lam MG, Viergever MA, de Jong HW. Feasibility of imaging 90Y microspheres at diagnostic activity levels for hepatic radioembolization treatment planning. Med Phys. 2020;47:1105–14.
47. Chiesa C, Maccauro M. 166 ho microsphere scout dose for more accurate radioembolization treatment planning. Eur J Nucl Med Mol Imag. 2020;47:744–7.
48. Chiesa C, Mira M, Maccauro M, Romito R, Spreafico C, Sposito C, Bhoori S, Morosi C, Pellizzari S, Negri A, Civelli E, Lanocita R, Camerini T, Bampo C, Carrara M, Seregni E, Marchianò A, Mazzaferro V, Bombardieri E. A dosimetric treatment planning strategy in radioembolization of hepatocarcinoma with 90Y glass spheres. Q J Nucl Med Mol Imaging. 2012;56(6):503–8.
49. Mazzaferro V, Sposito C, Bhoori S, Romito R, Chiesa C, Morosi C, Maccauro M, Marchianò A, Bongini M, Lanocita R, Civelli E, Bombardieri E, Camerini T, Spreafico C. Yttrium-90 radioembolization for intermediate-advanced hepatocellular carcinoma: a phase 2 study. Hepatology. 2012; https://doi.org/10.1002/hep.26014.
50. Kappadath SC, Mikell J, Balagopal A, Baladandayuthapani V, Kaseb A, Mahvash A. Hepatocellular carcinoma tumor dose response after 90Y-radioembolization with glass microspheres using 90Y-SPECT/CT-based voxel dosimetry. Int J Rad Oncol Biol Phys. 2018;102:451–61.
51. Walrand S, Hesse M, Chiesa C, Lhommel R, Jamar F. The low hepatic toxicity per gray of 90Y glass microspheres is linked to their transport in the arterial tree favoring a nonuniform trapping as observed in posttherapy PET imaging. J Nucl Med. 2014;55:135–40.
52. Walrand S, Hesse M, Jamar F, Lhommel R. A hepatic dose-toxicity model opening the way toward individualized radioembolization planning. J Nucl Med. 2014;55:1317–22.
53. Crookston NR, Fung GS, Frey EC. Development of a customizable hepatic arterial tree and particle transport model for use in treatment planning. IEEE Trans Radiat Plasma Med Sci. 2018;3:31–7.
54. d'Abadie P, Hesse M, Jamar F, Lhommel R, Walrand S. ^{90}Y TOF-PET based EUD reunifies patient survival prediction in resin and glass microspheres radioembolization of HCC tumours. Phys Med Biol 2018;63:245010.
55. Menda Y, Madsen MT, O'Dorisio TM, Sunderland JJ, Watkins GL, Dillon JS, Mott SL, Schultz MK, Zamba GK, Bushnell DL, O'Dorisio MS. 90Y-DOTATOC dosimetry–based personalized peptide receptor radionuclide therapy. J Nucl Med. 2018;59:1692–8.
56. Walrand S, Jamar F, van Elmbt L, Lhommel R, Bekonde EB, Pauwels S. 4-step renal dosimetry dependent on cortex geometry applied to 90Y peptide receptor radiotherapy: evaluation using a fillable kidney phantom imaged by 90Y PET. J Nucl Med. 2010;51:1969–73.
57. Smits ML, Nijsen JF, van den Bosch MA, Lam MG, Vente MA, Mali WP, van Het Schip AD, Zonnenberg BA. Holmium-166 radioembolisation in patients with unresectable, chemorefractory liver metastases (HEPAR trial): a phase 1, dose-escalation study. Lancet Oncol. 2012;13(10):1025–34.
58. van Roekel C, Bastiaannet R, Smits ML, Bruijnen RC, Braat AJ, de Jong HW, Elias SG, Lam MG. Dose-effect relationships of holmium-166 radioembolization in colorectal cancer. J Nucl Med. 2020;26:120.
59. Stella M, Braat AJ, Lam MG, de Jong HW, van Rooij R. Quantitative 166Ho-microspheres SPECT derived from a dual-isotope acquisition with 99mTc-colloid is clinically feasible. EJNMMI Phys. 2020;7:48.
60. Woliner-van der Weg W, Schoffelen R, Hobbs RF, Gotthardt M, Goldenberg DM, Sharkey RM, Slump CH, van der Graaf WTA, Oyen WJG, Boerman OC, Sgouros G, Visser EP. Tumor and red bone marrow dosimetry: comparison of methods for prospective treatment planning in pretargeted radioimmunotherapy. Eur J Nucl Med Mol Imaging Phys. 2014;1:104.
61. Blakkisrud J, Løndalen A, Dahle J, Turner S, Holte H, Kolstad A, Stokke C. Red marrow–absorbed dose for non-hodgkin lymphoma patients treated with 177lu-lilotomab satetraxetan, a novel anti-cd37 antibody–radionuclide conjugate. J Nucl Med. 2017;58:55–61.
62. Santoro L, Mora-Ramirez E, Trauchessec D, Chouaf S, Eustache P, Pouget JP, Kotzki PO, Bardiès M, Deshayes E. Implementation of patient dosimetry in the clinical practice after targeted radiotherapy using [177 Lu-[DOTA0, Tyr3]-octreotate]. Eur J Nucl Med Mol Imaging Research. 2018;8:103.

63. Garske-Roman U, Sandström M, Fröss Baron K, Lundin L, Hellman P, Welin S, Johansson S, Khan T, Lundqvist H, Eriksson B, Sundin A, Granberg D. Prospective observational study of 177Lu-DOTA-octreotate therapy in 200 patients with advanced metastasized neuroendocrine tumours (NETs): feasibility and impact of a dosimetry-guided study protocol on outcome and toxicity. Eur J Nucl Med Mol Imaging. 2018;45:970–88.
64. Hagmarker L, Svensson J, Rydén T, van Essen M, Sundlöv A, Gleisner KS, Gjertsson P, Bernhardt P. Bone marrow absorbed doses and correlations with hematologic response during 177Lu-DOTATATE treatments are influenced by image-based dosimetry method and presence of skeletal metastases. J Nucl Med. 2019;60:1406–13.
65. EW price. Synthesis, evaluation, and application of new ligands for radiometal based radiopharmaceuticals. 2014. Thesis. University British Columbia. https://open.library.ubc.ca/cIRcle/collections/ubctheses/24/items/1.0103411
66. Hamilton DH, Turcot I, Stintzi A, Raymond KN. Large cooperativity in the removal of iron from transferrin at physiological temperature and chloride ion concentration. JBIC J Biol Inorg Chem. 2004;9:936–44.
67. Bates GW, Billups C, Saltman P. THE kinetics and mechanism of iron (III) exchange between chelates and transferrin II. THE PRESENTATION AND REMOVAL WITH ETHYLENEDIAMINETETRAACETATE. J Biol Chem. 1967;242:2816–21.
68. Lubberink M, Wilking H, Öst A, Ilan E, Sandström M, Andersson C, Fröss-Baron K, Velikyan I, Sundin A. In vivo instability of 177Lu-DOTATATE during peptide receptor radionuclide therapy. J Nucl Med. 2020;61:1337–40.
69. https://www.ema.europa.eu/en/documents/product-information/lutathera-epar-product-information_en.pdf
70. Ilan E, Sandström M, Wassberg C, Sundin A, Garske-Román U, Eriksson B, Granberg D, Lubberink M. Dose response of pancreatic neuroendocrine tumors treated with peptide receptor radionuclide therapy using ^{177}Lu-DOTATATE. J Nucl Med. 2015;56:177–82.
71. D'Arienzo M, Cozzella ML, Fazio A, De Felice P, Iaccarino G, D'Andrea M, Ungania S, Cazzato M, Schmidt K, Kimiaei S, Strigari L. Quantitative 177Lu SPECT imaging using advanced correction algorithms in non-reference geometry. Phys Med. 2016;32:1745–52.
72. Rydén T, Heydom Lagerlöf J, Hemmingsson J, Marin I, Svensson J, Bath M, Gjertsson P, Bernhardt P. Fast GPU-based Monte Carlo code for SPECT/CT reconstructions generates improved ^{177}Lu images. Eur J Nul Med Mol Imaging Phys. 2018;5:1.
73. Ryden T, van Essen M, Marin I, Svensson J, Bernhardt P. Deep learning generation of synthetic intermediate projections improves ^{177}Lu SPECT images reconstructed with sparsely acquired projections. J Nucl Med. 2021;62(4):528–35.
74. Gregory RA, Murray I, Gear J, Leek F, Chittenden S, Fenwick A, Wevertt J, Scuffham J, Tipping J, Murby B, Jeans S, Stuffins M, Michopoulou S, Guy M, Morgan D, Hallam A, Hall D, Polydor H, Brown C, Gillen G, Dickinson N, Brown S, Wadsley J, Flux G. Standardized quantitative radioiodine SPECT/CT imaging for multicenter dosimetry trials in molecular radiotherapy. Phys Med Biol. 2019;64:245013.
75. Dewaraja YK, Schipper MJ, Shen J, Smith LB, Murgic J, Savas H, Youssef E, Regan D, Wilderman SJ, Roberson PL, Kaminski MS. Tumor-absorbed dose predicts progression-free survival following 131I-tositumomab radioimmunotherapy. J Nucl Med. 2014;55:1047–53.
76. Benabdallah N, Bernardini M, Biancardi M, de Labriolle-Vaylet C, Franck D, Desbrée A. ^{223}Ra-dichloride therapy of bone metastasis: optimization of SPECT images for quantification. Eur J Nucl Med Mol Imaging Res 2019;9:20.
77. https://en.wikipedia.org/wiki/Asepsis
78. https://en.wikipedia.org/wiki/Timeline_of_peptic_ulcer_disease_and_Helicobacter_pylori
79. Cremonesi M, Ferrari ME, Bodei L, Chiesa C, Sarnelli A, Garibaldi C, Pacilio M, Strigari L, Summers PE, Orecchia R, Grana CM. Correlation of dose with toxicity and tumour response to 90 Y-and 177 Lu-PRRT provides the basis for optimization through individualized treatment planning. Eur J Nucl Med Mol Imag. 2018;45:2426–41.
80. Sundlöv A, Sjögreen-Gleisner K. Peptide receptor radionuclide therapy–prospects for personalised treatment. Clin Oncol. 2021;33(2):92–7.
81. Cremonesi M, Ferrari M, Botta F. Dosimetry in PRRT. In: Clinical applications of nuclear medicine targeted therapy. Springer International Publishing; 2018. p. 297–313.
82. https://www.icrp.org/page.asp?id=10
83. Giammarile F, Muylle K, Bolton RD, Kunikowska J, Haberkorn U, Oyen W. Dosimetry in clinical radionuclide therapy: the devil is in the detail. Eur J Nucl Med Mol Imag. 2017;44:1–3.
84. Levillain H, Derijckere ID, Ameye L, Guiot T, Braat A, Meyer C, Vanderlinden B, Reynaert N, Hendlisz A, Lam M, Deroose CM. Personalised radioembolization improves outcomes in refractory intra-hepatic cholangiocarcinoma: a multicenter study. Eur J Nucl Med Mol Imag. 2019;46:2270–9.
85. Garin E, Tselikas L, Guiu B, Chalaye J, Edeline J, de Baere T, Assenat E, Tacher V, Robert C, Terroir-Cassou-Mounat M, Mariano-Goulart D. Personalised versus standard dosimetry approach of selective internal radiation therapy in patients with locally advanced hepatocellular carcinoma (DOSISPHERE-01): a randomised, multicentre, open-label phase 2 trial. Lancet Gastroenterol Hepatol. 2021;6(1):17–29.

86. Del Prete M, Buteau FA, Arsenault F, Saighi N, Bouchard LO, Beaulieu A, Beauregard JM. Personalized 177 Lu-octreotate peptide receptor radionuclide therapy of neuroendocrine tumours: initial results from the P-PRRT trial. Eur J Nucl Med Mol Imag. 2019;46:728–42.
87. Sundlöv A, Sjögreen-Gleisner K, Svensson J, Ljungberg M, Olsson T, Bernhardt P, Tennvall J. Individualised 177 Lu-DOTATATE treatment of neuroendocrine tumours based on kidney dosimetry. Eur J Nucl Med Mol Imag. 2017;44:1480–9.
88. Konijnenberg M, Herrmann K, Kobe C, Verburg F, Hindorf C, Hustinx R, Lassmann M. EANM position paper on article 56 of the council directive 2013/59/Euratom (basic safety standards) for nuclear medicine therapy. Eur J Nucl Med Mol Imaging. 2020;15:1–6.
89. Todd RW, Nightingale JM, Everett DB. A proposed γ camera. Nature. 1974;251:132–4.
90. Zaidi H, Sgouros G, editors. Therapeutic applications of Monte Carlo calculations in nuclear medicine. 2nd ed. CRC Press; 2002.
91. Buzhan P, Dolgoshein B, Ilyin A, Kantserov V, Kaplin V, Karakash A, Pleshko A, Popova E, Smirnov S, Volkov Y, Filatov L. The advanced study of silicon photomultiplier. In: Advanced technology and particle physics; 2002. p. 717–28.
92. Fujieda K, Kataoka J, Mochizuki S, Tagawa L, Sato S, Tanaka R, Matsunaga K, Kamiya T, Watabe T, Kato H, Shimosegawa E. First demonstration of portable Compton camera to visualize 223-Ra concentration for radionuclide therapy. Nucl Instrum Methods Phys Res Sect A: Accel Spectrom Detect Assoc Equip. 2020;958:162802.
93. Lee T, Kim M, Lee W, Kim B, Lim I, Song K, Kim J. Performance evaluation of a Compton SPECT imager for determining the position and distribution of 225Ac in targeted alpha therapy: a Monte Carlo simulation based phantom study. Appl Radiat Isot. 2019;154:108893.
94. Nagao Y, Yamaguchi M, Watanabe S, Ishioka NS, Kawachi N, Watabe H. Astatine-211 imaging by a Compton camera for targeted radiotherapy. Appl Radiat Isot. 2018;139:238–43.